nature communications

Article

https://doi.org/10.1038/s41467-025-64739-7

Chiral macrocycles forming high-affinity host-guest homoternary complexes for chiral discrimination and amplified circularly polarized luminescence

Received: 13 February 2025

Accepted: 23 September 2025

Published online: 04 November 2025

Check for updates

Rong Fu[1,2], Fang-Yuan Chen[1,3], Le Dai[4], Dai-Yuan Li[1], Qing-Yu Zhao[1], Si-Dan Guo[1,3], Zi-Hang Song[1], Li-Bo Jing[1], Heng Wang[4,5], Xiaopeng Li[4,5,6], Dong-Sheng Guo[1,3,7] & Kang Cai[1]

The development of macrocyclic hosts with high-affinity 1:2 recognition capabilities is crucial for advancing supramolecular chemistry and its applications. While cucurbit[8]uril (CB[8]) has long been recognized for its unparallel 1:2 binding affinity, its limitations—including poor solubility, difficulty to modify and lack of optical activity—have hindered broader utilization. Here, we introduce a class of enantiopure chiral macrocycles, *RRRR*- or *SSSS*-corral[4]BINOL (C[4]Bs), which exhibit remarkable 1:2 recognition properties in water that are comparable or even surpass CB[8]. Using UV-Vis, fluorometric, and isothermal titration calorimetry (ITC), we demonstrate that C[4]Bs form stable homoternary complexes with 11 singly positively charged planar aromatic guests, with binding affinities up to $10^{17}\,M^{-2}$. These ultrahigh affinities make C[4]Bs versatile alternatives to CB[8], offering advantages such as superior water-solubility, ease of structural modification, and strong fluorescence. Furthermore, the unique chiral nature of C[4]Bs enables efficient fluorescent discrimination of chiral substrates and chirality transfer to non-chiral dyes, resulting in strong circularly polarized luminescence (CPL) with $|g_{lum}|$ values up to 1.1×10^{-2}. This study establishes C[4]Bs not only as powerful hosts for aqueous-phase supramolecular complexation but also as a promising platform for developing chiral functional materials.

The dynamic reversibility of non-covalent recognition interactions renders them inherently concentration-dependent, highlighting the importance of binding affinity in ensuring the practical applicability of recognition pairs across a wide concentration range[1]. Despite the extensive development of supramolecular macrocyclic systems over recent decades, cucurbit[*n*]urils (CB[*n*]s), particularly CB[7] and CB[8], remain irreplaceable in host-guest chemistry on account of their exceptional binding strength in aqueous solutions[2–5]. CB[7] exhibits 1:1

[1]College of Chemistry, State Key Laboratory of Elemento-Organic Chemistry, Frontiers Science Center for New Organic Matter, Nankai University, Tianjin, China. [2]College of Environmental Science and Engineering, Nankai University, Tianjin, China. [3]Key Laboratory of Functional Polymer Materials (Ministry of Education), Collaborative Innovation Center of Chemical Science and Engineering, Nankai University, Tianjin, China. [4]State Key Laboratory of Organometallic Chemistry, Shanghai Institute of Organic Chemistry, University of Chinese Academy of Sciences, Chinese Academy of Sciences, Shanghai, China. [5]College of Chemistry and Environmental Engineering, Shenzhen University, Shenzhen, Guangdong, China. [6]Shenzhen University General Hospital, Shenzhen University Clinical Medical Academy, Shenzhen, Guangdong, China. [7]Xinjiang Key Laboratory of Novel Functional Materials Chemistry, College of Chemistry and Environmental Sciences, Kashi University, Kashi, China. e-mail: kangcai@nankai.edu.cn

binding affinities exceeding $10^9\,M^{-1}$, with the strongest interactions reaching up to $10^{17}\,M^{-1}$ [6]. CB[8] not only shows high 1:1 affinity but also forms 1:2 host-guest complexes, with affinities as high as $10^{16}\,M^{-2}$ [7]. This remarkable ability to recognize both 1:1 and 1:2 complexes in water and their biocompatibility positions CB[*n*]s as superior hosts compared to other macrocycles, leading to their widespread application in many different research fields[8].

Achieving high-affinity recognition requires excellent structural complementarity between host and guest, maximizing interactions while minimizing entropic penalties to overcome the limitations of enthalpy–entropy compensation[4,9–11]. For 1:2 binding, the design of host-guest complementarity poses even greater challenges than for 1:1 binding, as the formation of tightly bounded ternary complexes demands heightened structural complementarity and inevitably incurs larger entropic losses. Consequently, while recent advances have yielded several novel macrocyclic hosts with high 1:1 binding affinities exceeded nanomolar level[12–25], replicating the 1:2 recognition capabilities of CB[8] remain a significant challenge.

The importance of high-affinity 1:2 binding hosts lies in their ability to serve as robust yet dynamic noncovalent linkers for efficient molecular conjugation technologies, which are highly useful in polymer chemistry[26–29], nanotechnology[30,31], and biomedicine[32–34]. For example, CB[8] has proven itself as a robust noncovalent connector, by linking guest-modified partners—such as small molecules, macromolecules, nanoparticles, and surfaces—with high-fidelity and stimuli-responsiveness. This versatility underpins its widespread use in supramolecular polymers[35–43], hydrogels[44–46], bioorthogonal labeling[47], nanoparticle assembly[48], and surface modifications[49]. Despite its well-known limitations—including poor solubility[50] (water solubility <0.1 mM), difficulty in modification, and lack of optical activity—CB[8]'s unmatched 1:2 recognition capability remains indispensable in many studies (Fig. 1). This underscores the urgent need for new macrocyclic hosts that not only provide high-affinity 1:2 recognition[51–58] but also offer additional advantages, thus expanding the toolbox of supramolecular chemistry and unlocking new, versatile applications across various fields.

In our previous work[59–62], we have developed a new class of water-soluble, enantiopure chiral macrocycles, namely *RRRR*- or *SSSS*-corral[4]BINOL (*R*- or *S*-C[4]B)[59,60]. With their deep, nonpolar, chiral cavity, C[4]Bs exhibit exceptionally high 1:1 recognition affinities for a range of hydrophobic guests, such as steroidal compounds. Given that their cavity width (approximately 7.1 Å) and volume (389 Å^3) are comparable to CB[8], we hypothesized that they could also achieve high-affinity 1:2 recognition. In this study, we systematically investigated the 1:2 recognition properties of C[4]Bs using isothermal titration calorimetry (ITC), UV-Vis, and fluorometric titrations. The results revealed that C[4]Bs' high 1:2 binding affinity (ranging from 10^9 to $10^{17}\,M^{-2}$), even surpasses that of CB[8]. Moreover, C[4]Bs' excellent water solubility, modifiable structure, and strong fluorescent emission address the limitations of CB[8].

Theoretically, C[4]Bs can achieve most of the functions of CB[8], and even surpass them in many aspects. However, the most distinctive feature of C[4]Bs lies in their chiral nature, which significantly expands their functional possibilities. To demonstrate this, we showed that C[4]Bs facilitate efficient enantioselective 1:2 recognition of chiral guests and transfer chirality to non-chiral dyes, generating amplified circularly polarized luminescence (CPL) with $|g_{lum}|$ up to 1.1×10^{-2}, which is among the highest reported for chiral host-dye complexes. These findings establish C[4]Bs' not only as promising alternatives to CB[8], but also as a versatile platform for developing chiral functional materials.

Results and discussion

Determination of 1:2 binding affinities by titrations

The *RRRR*-corral[4]BINOL and *SSSS*-corral[4]BINOL used in the experiments were obtained using established synthetic procedures[60], the experimentally determined solubility was found to be >10 mM. Inspired by CB[8], we selected 11 singly positively charged planar aromatic compounds (Fig. 2) as potential guests for the formation of 1:2 host-guest complexes with C[4]Bs ($K_{12} = K_1 \times K_2$). To investigate the host-guest recognition, we primarily employed ITC titration, which provides clear and reliable information on binding stoichiometry and constants, along with thermodynamic parameters essential for elucidating the driving forces behind the recognition process. For certain guests, significant changes in fluorescence and UV-Vis spectra were observed, promoting us to use fluorometric and/or UV-Vis titrations in conjunction with ITC to further probe the host-guest interactions. By combining multiple titration techniques, we obtained robust evidence for the 1:2 host-guest recognition between C[4]Bs and the selected guests, enhancing the reliability of our binding constant determinations. All experiments were conducted in 10 mM PBS buffer to minimize pH-related variations and complexities.

As an example, thioflavine T (ThT), a well-known fluorescent dye, was titrated into a *R*-C[4]B solution in phosphate buffer saline (PBS) buffer (Fig. 3). The ITC titration curve (Fig. 3b, c) revealed two distinct transitions, suggesting the formation of a homoternary complex (*R*-C[4]B@2ThT). Fitting the data to a sequential binding model yielded the following binding constants: $K_1 = (5.4 \pm 1.5) \times 10^8\,M^{-1}$, $K_2 = (2.4 \pm 0.6) \times 10^6\,M^{-1}$, and the overall binding constant, $K_{12} = 1.3 \times 10^{15}\,M^{-2}$. Both K_1 and K_2 were found to be driven by a favorable enthalpic hydrophobic effect, particularly for K_2. UV-Vis titrations (Fig. 3d, e) further confirmed the high-affinity 1:2 complexation. Upon titrating *R*-C[4]B into a ThT solution (10 μM), the absorption band of ThT redshifted from 412 to 430 nm, with a well-defined isosbestic point at 425 nm. On further addition of *R*-C[4]B, the absorption peak continued to redshift to 451 nm, with a second isosbestic point appearing at 438 nm. These two consecutive isosbestic points confirmed the two-step binding process (1:1 and 1:2 complexes) and provided a $K_{12} = 4.2 \times 10^{15}\,M^{-2}$, with $K_1 = (1.5 \pm 0.7) \times 10^9\,M^{-1}$ and $K_2 = (2.8 \pm 0.8) \times 10^6\,M^{-1}$ by fitting to a 1:2 host-guest binding model. Fluorometric titrations further supported the 1:2 recognition between *R*-C[4]B and ThT. A noticeable two-stage fluorescence enhancement was observed (Fig. 3f, g) upon gradually adding *R*-C[4]B to a 2.0 μM ThT solution. The binding of ThT to the host restricts the dye's rotational and vibrational motions, significantly reducing non-radiative deactivation pathways, thereby dramatically enhancing the fluorescence. By tracking the fluorescent intensity at 600 nm and fitted to a 1:2 host-guest binding model, the binding affinities of the *R*-C[4]B@2ThT complex were determined to be $K_{12} = 2.8 \times 10^{15}\,M^{-2}$, with $K_1 = (9.3 \pm 0.4) \times 10^8\,M^{-1}$ and $K_2 = (3.0 \pm 0.7) \times 10^6\,M^{-1}$. Thus, the three titration methods (ITC, UV-Vis, and fluorescence) consistently demonstrate the two distinct binding stages (1:1 and 1:2 complexation) between *R*-C[4]B and ThT, with highly consistent binding constants across all techniques.

The exceptional binding affinity of *R*-C[4]B for ThT has prompted further investigation into its 1:2 recognition ability with a diverse range of ten additional guests, including two quaternary ammonium salts (G1 and G2), six pyridinium salts (G3–G8), and two organic dyes, methylene blue (MB) and thiazole orange (TO), as depicted in Figs. S20–S40. Binding constants for nine of these guests were determined using isothermal titration calorimetry (ITC), with the exception of G1, which was characterized using fluorometric titrations. For G7 and MB, UV-Vis titrations were also employed, while TO was additionally investigated by fluorometric titrations to cross-validate the results. All titration data are summarized in Table 1. The results reveal that for the two quaternary ammonium salts (G1 and G2), K_{12} values range between 10^9 and $10^{10}\,M^{-2}$. For three 4-phenylpyridinium salts (G3–G5), K_{12} values are consistently in the range of $10^{11}\,M^{-2}$, while for the three 4-styrylpyridinium derivatives (G6–G8), K_{12} are even higher, ranging from 10^{12} to $10^{14}\,M^{-2}$. Notably, these binding affinities are comparable to those reported for CB[8] with similar guests. Surprisingly, the K_{12}

https://doi.org/10.1038/s41467-025-64739-7

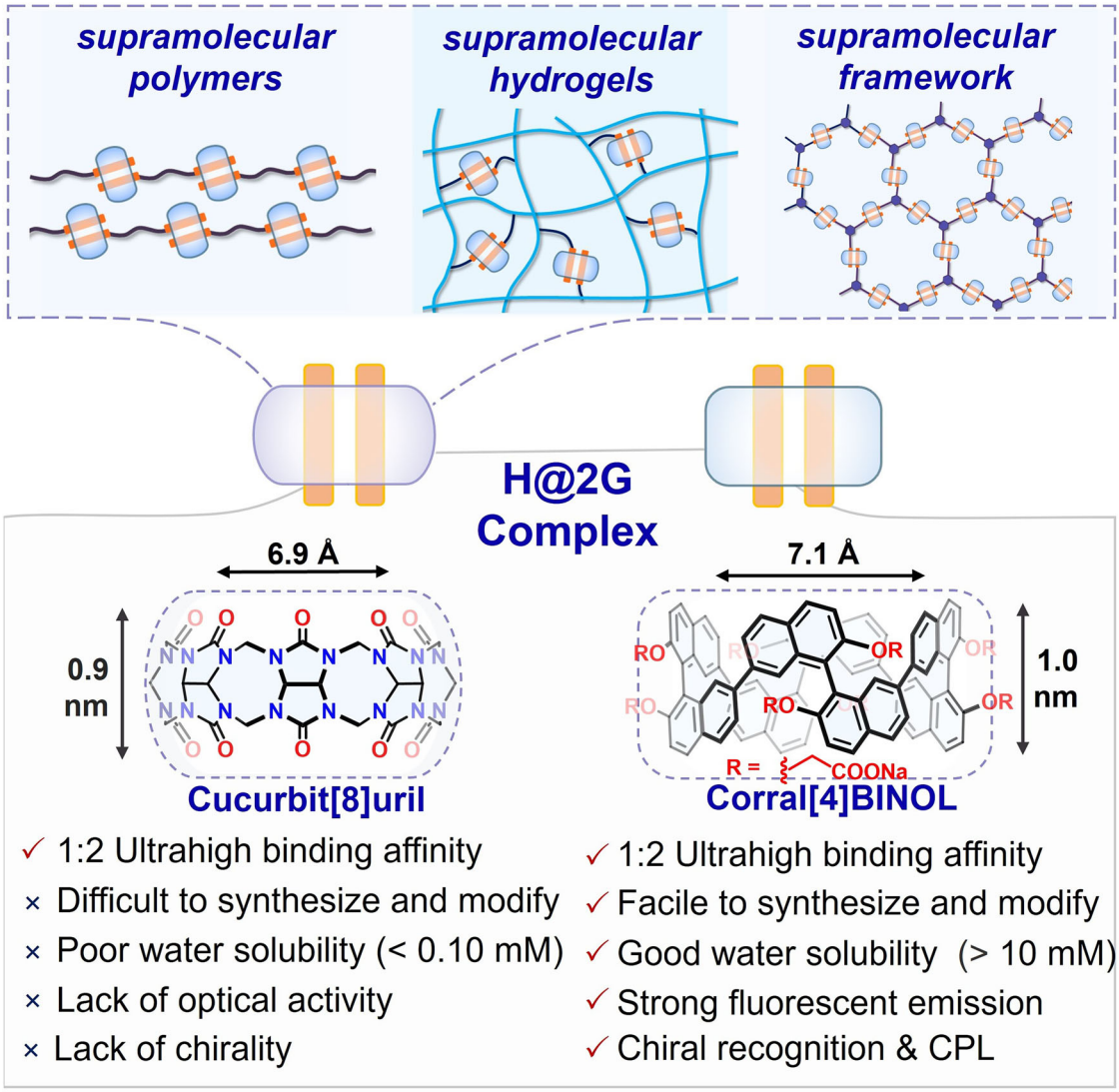

Fig. 1 | Schematic illustration. Schematic representation of the application of the host@2guest (H@2G) complex in supramolecular polymers, hydrogels, and organic frameworks. And a comparative analysis of the characteristics of cucurbit[8]uril (CB[8]) and corral[4]BINOL (C[4]B), both exhibiting 1:2 binding capability.

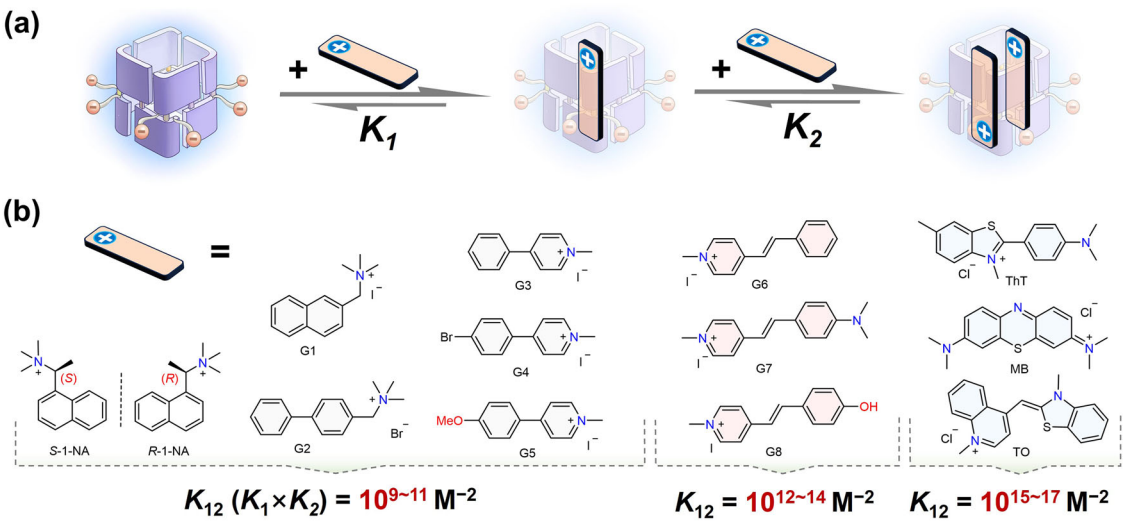

Fig. 2 | Investigation of the 1:2 complexation behavior between *R*-C[4]B and selected analytes. a Schematic illustration of the formation process of *R*-C[4]B@2guest homoternary complex. **b** Structures of selected analytes and ranges of binding constants with *R*-C[4]B in PBS buffer solution.

https://doi.org/10.1038/s41467-025-64739-7

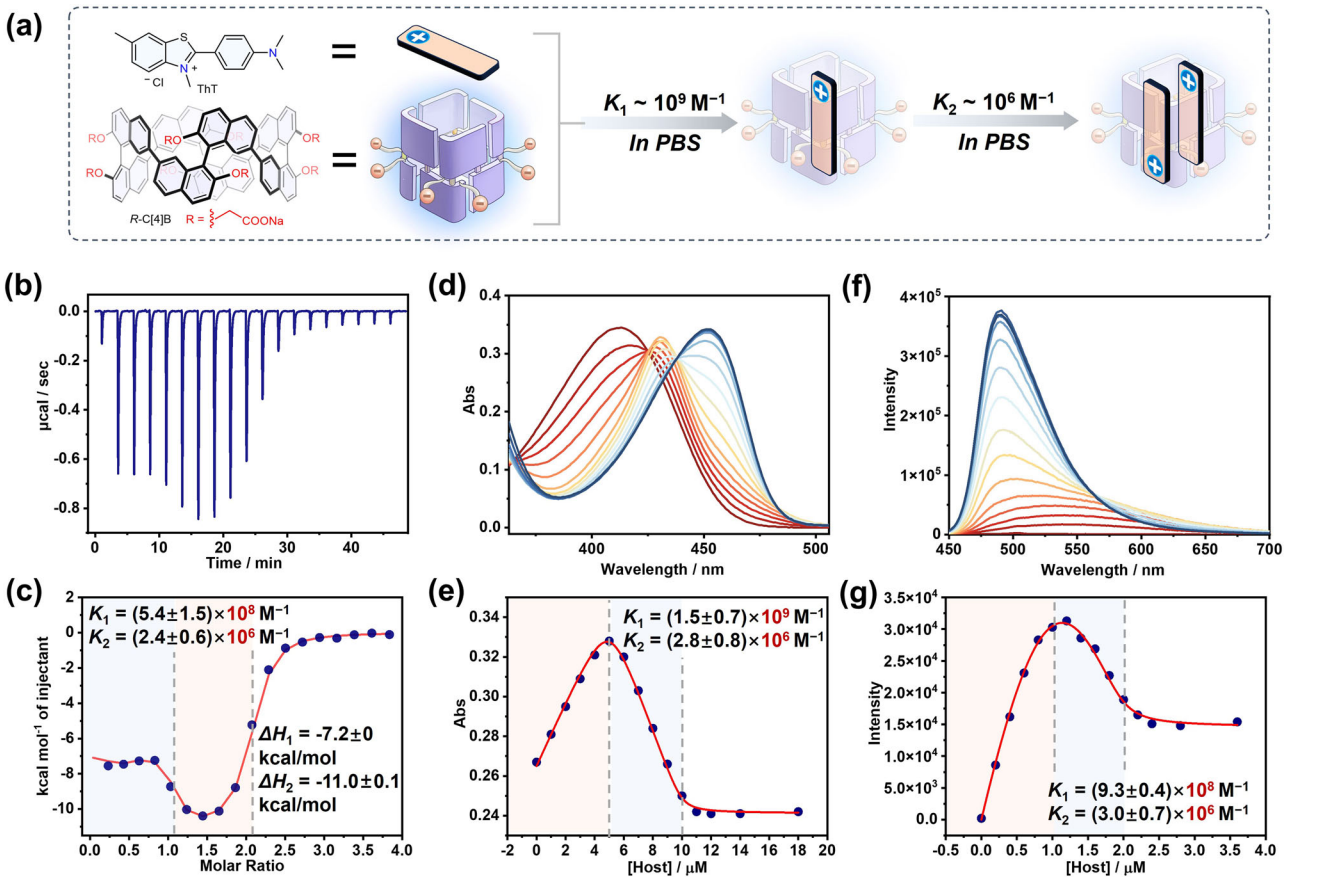

Fig. 3 | Investigation of the 1:2 complexation behavior between *R*-C[4]B and ThT in 10 mM PBS buffer solution. a Schematic illustration of *R*-C[4]B@2ThT homoternary complex. **b** Isothermal titration calorimetry (ITC) isotherms obtained by adding ThT (800 μM) into a 19.5 μM solution of *R*-C[4]B at 25 °C. **c** The analyzed data of ITC isotherms with the sequential binding model. **d** UV-Vis titration spectra obtained by adding *R*-C[4]B (up to 18 μM) into a 10.0 μM solution of ThT. **e** The fitting curve plot by tracking absorbance at λ = 430 nm. **f** Fluorometric titration spectra obtained by adding *R*-C[4]B (up to 3.6 μM) into a 2.0 μM solution of ThT. **g** The fitting curve plot by tracking emission intensity at λ = 600 nm, with the nonlinear curve fitting by using 1:2 host-guest binding model. The binding constant is the average of two experiments and the error indicated is the calculated standard deviation.

values for *R*-C[4]B with MB and TO reach e $4.9 \times 10^{16}\,M^{-2}$ (UV-Vis titration) and $1.7 \times 10^{17}\,M^{-2}$ (UV-Vis titration). To the best of our knowledge, these values represent the highest binding affinities reported for 1:2 ternary host-guest complexes[2].

Thermodynamic analysis, as summarized in Table 1 and Table S1, provides further insights into the complexation mechanism for each guest. Across all binding processes, the free energies (ΔG) are predominantly driven by highly favorable enthalpic contributions, indicating that non-classical hydrophobic interactions are the primary driving force. Additionally, a substantial entropic contribution is observed in K_1, similar to the findings with CB[8]. Structural analysis suggests that the increased entropy resulting from desolvation due to the large hydrophobic surface area of the dyes significantly enhances the binding process. Quantitative analysis of cooperativity was further conducted by using the interaction parameter ($\alpha = 4K_2/K_1$). When the value of log α is larger than 0.5, the system displays positive cooperativity; when log α is smaller than −0.5, the system displays negative cooperativity; and when log α is between −0.5 and 0.5, the system is noncooperative[63,64]. As Table 1 showed, G1, G4, ThT, MB, and TO exhibit negative cooperativity, while the others show noncooperative. Specifically, for ThT and TO systems, the observed negative cooperativity arises from an initial large entropy gain ($-T\Delta S_1 < -4.0$ kcal mol^{-1}) due to hydrophobic core burial, followed by a significant entropy penalty ($-T\Delta S_2 > 2.7$ kcal mol^{-1}) during the second guest binding. This two-stage thermodynamic profile aligns perfectly with established mechanisms of hydrophobic effect-driven negative cooperativity reported in prior studies[38,63,65–67].

NMR characterizations for the 1:2 homoternary complexes

NMR characterizations were performed to gain deeper structural insights into the 1:2 host-guest complexes in solutions. As a representative guest, G5 was selected to form a homoternary complex with *R*-C[4]B and characterized in D_2O using ^1H NMR. As shown in Fig. 4, the proton signals of G5 undergo dramatic upfield shifts upon complexing with *R*-C[4]B, compared to free guest, demonstrating a strong shielding effect exerted by the aromatic walls of the host. Specifically, the upfield shifts of the protons in G5 follow the order: $H_2 \approx H_3$ (3.0 − 3.2 ppm) > H_4 (2.5 ppm) » H_1 (1.6 ppm) » H_6 (0.68 ppm) > H_5 (0.51 ppm). This demonstrates varying degrees of shielding for each proton, which reflects their positions within the host cavity. The most strongly shielded protons, H_2 and H_3, are likely situated at the center of the cavity. This is further confirmed by ^1H-^1H nuclear overhauser effect spectroscopy (NOESY), which shows clear correlations between the host proton H_a and guest protons H_2 and H_3 (Fig. S3). Protons H_1 and H_5 in pyridinium unit exhibit smaller upfield shifts than the corresponding H_4 and H_6 in 4-methoxyphenyl unit, respectively, suggesting that the pyridinium unit is positioned further from the cavity's center compared to the 4-methoxyphenyl unit. This can be attributed to the more hydrophilic nature of the charged pyridinium unit, making it more exposed to the solvent.

https://doi.org/10.1038/s41467-025-64739-7

Table 1 | Binding affinities of *R*-C[4]B towards selected analytes determined by fluorometric (FL) titrations, UV-Vis (UV) titrations, and/or ITC titrations in PBS buffer solution, and schematic illustration of thermodynamic parameters

Guests	K_1 (M^{-1})[a]	K_2 (M^{-1})[b]	K_{12} (M^{-2})	logα	Method
G1	(2.4 ± 0.9) × 10^6	(1.5 ± 0.9) × 10^3	3.6 × 10^9	−2.6	FL
G2	(6.3 ± 0.1) × 10^5	(3.5 ± 1.1) × 10^5	2.2 × 10^{11}	0.35	ITC
G3	(4.2 ± 0.8) × 10^5	(5.7 ± 1.5) × 10^4	2.4 × 10^{10}	−0.27	ITC
G4	(2.1 ± 0.1) × 10^6	(1.6 ± 0.6) × 10^5	3.4 × 10^{11}	−0.52	ITC
G5	(2.1 ± 0.2) × 10^6	(2.9 ± 0.9) × 10^5	6.1 × 10^{11}	−0.26	ITC
G6	(3.2 ± 2.5) × 10^6	(1.6 ± 0) × 10^6	5.1 × 10^{12}	0.3	ITC
G7	(6.2 ± 1.3) × 10^5	(1.6 ± 0) × 10^7	9.9 × 10^{13}	1.0	FL
	(1.4 ± 0.2) × 10^7	(1.5 ± 0.5) × 10^6	2.1 × 10^{13}	−0.37	ITC
G8	(2.7 ± 0.8) × 10^7	(6.8 ± 0.8) × 10^6	1.8 × 10^{14}	0.0032	ITC
ThT	(9.3 ± 0.4) × 10^8	(3.0 ± 0.7) × 10^6	2.8 × 10^{15}	−1.9	FL
	(1.5 ± 0.7) × 10^9	(2.8 ± 0.8) × 10^6	4.2 × 10^{15}	−2.1	UV
	(5.4 ± 1.5) × 10^8	(2.4 ± 0.6) × 10^6	1.3 × 10^{15}	−1.8	ITC
MB	(8.8 ± 1.4) × 10^9	(5.6 ± 0.8) × 10^6	4.9 × 10^{16}	−2.6	UV
	(2.1 ± 1.1) × 10^9	(5.0 ± 0.9) × 10^6	1.0 × 10^{16}	−2.0	ITC
TO	(9.2 ± 1.6) × 10^9	(2.6 ± 0.6) × 10^8	2.4 × 10^{18}	−0.95	FL
	(3.4 ± 1.7) × 10^9	(4.9 ± 0.5) × 10^7	1.7 × 10^{17}	−1.2	UV
	(1.9 ± 0.1) × 10^9	(4.4 ± 2.1) × 10^7	8.4 × 10^{16}	−1.0	ITC
Thermodynamic parameters[b]					

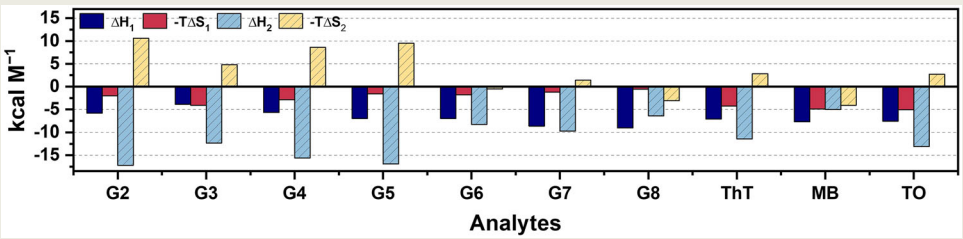

[a]Typical errors were determined by repeating the titrations twice and are presented as mean ± sd.
[b]Thermodynamic parameters ΔH_1, ΔH_2, $-T\Delta S_1$ and $-T\Delta S_2$ obtained from ITC titrations for *R*-C[4]B with selected guests in 10 mM PBS buffer.

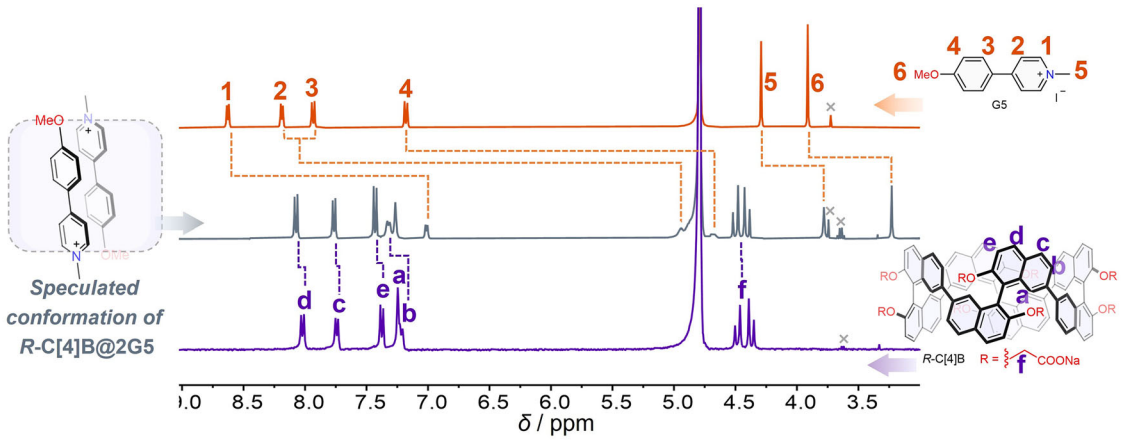

Fig. 4 | ^{1}H NMR spectra of host–guest complex. Top: 2.0 mM G5; Middle: 1:2 mixture of 1.0 mM *R*-C[4]B and 2.0 mM G5; Bottom: 1.0 mM *R*-C[4]B. (400 MHz, D_2O, 298 K).

Systematic NMR titration experiments were performed for all 11 guest molecules (Figs. S4–S14). The results demonstrate fast-exchange dynamics between C[4]B and most guests on the NMR timescale. Among all guests, only ThT and TO displayed slow-exchange behavior, likely due to their relatively stronger binding affinities. Additionally, the formation of 1:2 host-guest complexes was further confirmed by mass spectrometry analysis of *R*-C[4]B@2G1, *R*-C[4]B@2G2, *R*-C[4]B@2G4, *R*-C[4]B@2G7, and *R*-C[4]B@2ThT (Figs. S15–S19).

Based on these NMR data, we propose that the two G5 molecules in the *R*-C[4]B cavity adopt a slightly offset antiparallel stacking arrangement, as illustrated in the schematic. This antiparallel arrangement minimizes electrostatic repulsion and favors direct dipole–dipole interactions, while the slight offset allows the hydrophobic 4-methoxyphenyl groups to be fully encapsulated within the cavity, with the more hydrophilic pyridinium units exposed to the solvent. Further analysis of the ^{1}H NMR spectrum for the *R*-C[4]B@2G7 complex reveals

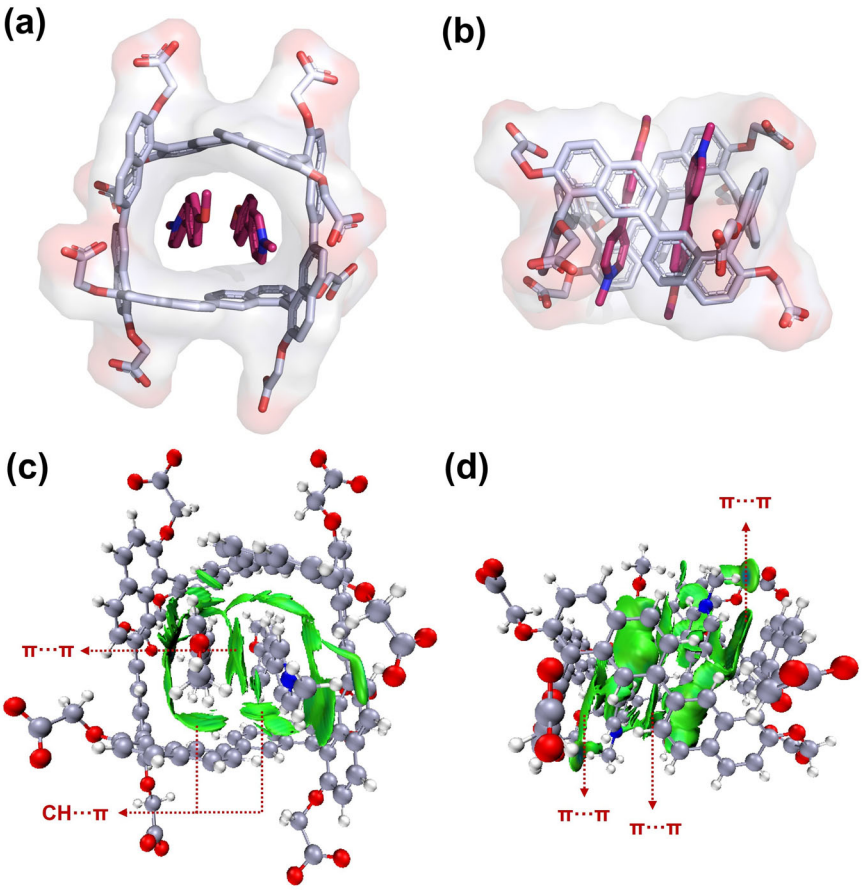

Fig. 5 | Calculated energy-minimized conformations of *R*-C[4]B@2G5 homoternary complex. a Top-down and **b** side-on views of the energy-minimized conformation of *R*-C[4]B@2G5 using DFT calculations at the B3LYP−D3/6-31G(d) level. **c** Top-down and **d** side-on views of the intermolecular binding isosurfaces of the *R*-C[4]B@2G5 obtained from an independent gradient model based on Hirshfeld partition (IGMH) analysis ($\rho = 0.004$ au).

a similar pattern of chemical shift changes (Fig. S1), supporting that G7 adopts the same binding mode as G5. Similar antiparallel stacking mode have also been observed in the homoternary complexes of CB[8]. These detailed NMR analyses provide critical evidence for the structural arrangement of the 1:2 host-guest complex, highlighting the strong interactions between *R*-C[4]B and its guests.

Energy-minimized conformations for the homoternary complexes

The energy-minimized conformations of *R*-C[4]B@2G5 homoternary complex was then calculated using density functional theory (DFT) method at the B3LYP-D3/631G(d) level (Fig. 5a, b)[68], and the corresponding independent gradient model based on Hirshfeld partition (IGMH) analysis (Fig. 5c, d) were also performed[69,70], in which interactions are expressed in green. The results indicate that the two guests are encapsulated in an antiparallel orientation within the cavity, aligning with the previously drawn conclusion. Notably, the weak interactions identified by IGMH analysis reveal varying interactions observed between the guests and the host cavity, involving the [π···π] interactions between the guest's aromatic rings and the aromatic wall on the host, and [CH···π] interactions between the hydrogen atoms on the guest's aromatic rings and the aromatic wall of *R*-C[4]B on the other side. Additionally, there are two distinct interaction patterns between the guests, [π···π] and [CH···π] interactions, indicate that the guests have formed H aggregates. Further energy-minimized conformations and IGMH analysis for the *R*-C[4]B@2G6 complex reveals a similar result (Fig. S45), supporting that G6 adopts the similar antiparallel stacking mode as G5.

Fluorescent discrimination of chiral guests

The unique chirality and fluorescence emission properties of C[4]Bs represent significant advantages over CB[8]. Building on this, we explored the potential of C[4]Bs for fluorescent discrimination of chiral guests through 1:2 host-guest complexation. As shown in Fig. 6a, the addition of *S*-1-NA to a solution of *S*-C[4]B resulted in an initial sharp increase in fluorescence intensity by 24%, followed by a gradual decrease. In contrast, the introduction of the other enantiomer, *R*-1-NA, led to an initial rapid decrease in fluorescence intensity by 18%, followed by a gradual decline (Fig. 6b). These distinct fluorescence responses highlight the enantioselective binding behavior of *S*-C[4]B. By monitoring the fluorescence intensity at 400 nm and fitting the data to a 1:2 host-guest binding model (Fig. 6c), the binding affinities of the *S*-C[4]B@2S-1-NA and *S*-C[4]B@2R-1-NA complexes were determined to be $K_{12} = 1.1 \times 10^{10}\,M^{-2}$ and $K_{12} = 3.0 \times 10^{9}\,M^{-2}$, respectively, with an enantioselectivity (α) value of 3.5. The binding constants and enantiomeric selectivity of the other chiral host, *R*-C[4]B, further validate the robustness of these results, as demonstrated in Figs. S25–S26. The remarkable 1:2 chiral recognition capabilities of C[4]Bs, combined with their distinctive fluorescence response characteristics, underscore their significant potential for further exploration and development in the field of chiral sensing.

Chiral transfer and CPL amplification upon 1:2 complexing

The transfer of chirality from chiral macrocycles to achiral dyes through host-guest interactions presents an attractive strategy for inducing chiroptical properties, such as circular dichroism (CD) and circularly polarized luminescence (CPL) signals, in achiral dyes[58,71–77].

https://doi.org/10.1038/s41467-025-64739-7

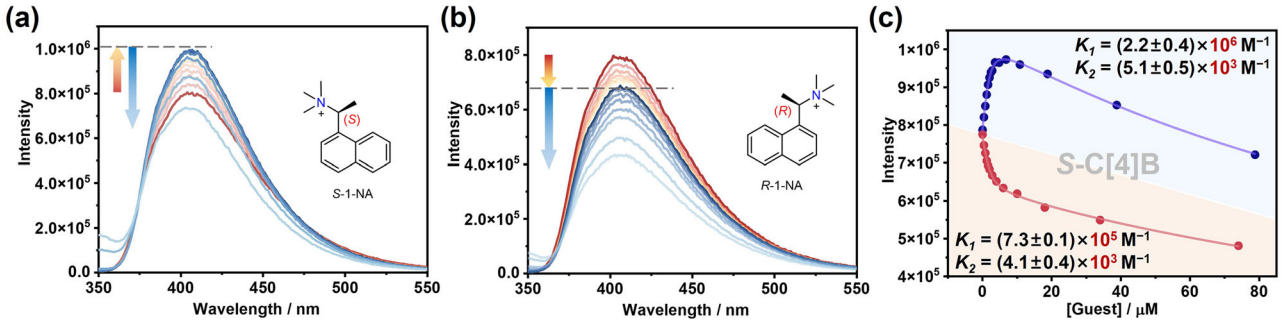

Fig. 6 | The fluorescent discrimination of chiral guests *S*-1-NA and *R*-1-NA upon 2:1 complexing with *S*-C[4]B. a Changes in fluorescence spectrum of 2.0 μM *S*-C[4]B upon addition of *S*-1-NA (up to 80 μM). **b** Changes in fluorescence spectrum of 2.0 μM *S*-C[4]B upon addition of *R*-1-NA (up to 74 μM). **c** The fitting curve plot of *S*-C[4]B upon addition of *S*-1-NA and *R*-1-NA for emission at λ = 400 nm, according to the nonlinear curve fitting with 1:2 host-guest binding model.

However, examples of host-guest complexes involving chiral macrocycles, such as cyclodextrins[78] or helic[6]arenes[79,80], with dyes to generate CPL in solution have typically reported relatively low luminescence dissymmetry factors ($|g_{lum}|$) in the range of 10^{-4} to 10^{-3}. Given that C[4]Bs can form stable 1:1 and 1:2 complexes with dyes such as ThT and TO, we explored the potential for chirality transfer from C[4]Bs to these guest dyes via host-guest recognition. Therefore, we prepared aqueous solutions of *R*- and *S*-C[4]Bs with ThT and TO to form 1:1 and 1:2 host-guest complexes and measured their CD and CPL spectra.

As shown in Fig. 7b, f, the free *R*- and *S*-C[4]B display CD signals below 400 nm, while both free ThT and TO are CD-silent. However, upon forming 1:1 and 1:2 complexes with *R*- and *S*-C[4]B, new CD signals emerge above 400 nm, corresponding to the absorption regions of ThT and TO. The CD signals of the *R*- and *S*-C[4]B complexes are mirror-image symmetric, indicating effective chirality transfer from the chiral host to the achiral dye in their ground state. Notably, the CD signals of both the host C[4]B and the guests (ThT or TO) in 1:2 complexes are significantly stronger than in 1:1 complexes, indicating that binding two guests imposes greater conformational constraints on the host. This enhances the host's CD signal and facilitates more effective chiral transfer[54,78] from host to guest in 1:2 complexes compared to 1:1 complexes.

We also measured the fluorescence spectra of the four host-guest complexes. As shown in Fig. 7c, g, both ThT and TO are typical TICT (twisted intramolecular charge transfer) dyes, exhibiting very weak fluorescence in aqueous solution. However, upon complexation with *R*-C[4]B to form 1:1 and 1:2 complexes, the fluorescence intensity of both dyes increased significantly. For example, the fluorescence intensity of *R*-C[4]B@ThT was enhanced by 386-fold compared to free ThT, and *R*-C[4]B@2ThT showed a 67-fold increase. Similarly, for TO, the fluorescence increase was more significant for the 1:2 complex compared to the 1:1 complex. These results suggest that the hydrophobic cavity of *R*-C[4]B significantly enhances the fluorescence emission of both ThT and TO, likely due to the restriction of their motion within the host cavity.

We further examined the CPL spectra of the four host-dye complexes. As shown in Figs. 7d and S41, the CPL signals for both *R*-C[4]B@ThT and *S*-C[4]B@ThT exhibit mirror-image Cotton effects with peaks at 490 nm and a luminescence dissymmetry factor ($|g_{lum}|$) of 1.3×10^{-3}. In contrast, the 1:2 complexes, *R*-C[4]B@2ThT and *S*-C[4]B@2ThT, display mirror-image Cotton effects at 560 nm with a significantly enhanced $|g_{lum}|$ of 5.0×10^{-3}, which is 3.6 times higher than that of the host alone ($|g_{lum}| = 1.4 \times 10^{-3}$). Notably, the CPL signals for the 1:1 complexes of TO (*R*-C[4]B@TO and *S*-C[4]B@TO) were negligible. However, for the 1:2 complexes, *R*-C[4]B@2TO and *S*-C[4]B@2TO, a high $|g_{lum}|$ value of 1.1×10^{-2} was observed, surpassing the free host by 7.8 times, as shown in Figs. 7h and S42. This represents one of the highest $|g_{lum}|$ values reported for chiral host-guest complexes in solution. These results demonstrate that the 1:2 complexes exhibit stronger CPL induction and greater enhancement compared to the 1:1 complexes. This is likely due to the more restricted conformational motion of the dyes in the 1:2 complexes, facilitating more efficient chirality transfer and thus yielding a higher CPL dissymmetry factor. However, given the conformational dynamics and structural complexity of the ternary supramolecular system in solution, elucidating the clear structure-property relationship governing chirality transfer/amplification within the C[4]B cavity remains a significant challenge.

Therefore, the binding of two achiral dyes to *R*- or *S*-C[4]B not only dramatically enhances their fluorescent emission but also induces notable chiral photophysical properties. It is important to note that the assembly of the ThT and TO homoternary complexes was achieved at a relatively low concentration (10 μM), owing to the high binding affinity (ranging from 10^{15} to $10^{17}\,M^{-2}$) that ensures stable 1:2 complex formation. This high affinity makes these complexes versatile and applicable across a range of concentrations for potential applications—such as bioimaging and biosensing—in solution phase. Thus, *R*- or *S*-C[4]B-based 1:2 homoternary complexes provide an excellent platform for constructing various CPL materials with tunable properties.

In conclusion, we have thoroughly explored the 1:2 complexation properties of the emerging chiral macrocycle corral[4]BINOLs (C[4]Bs) with 11 singly positively charged planar aromatic guests. Through a combination of various titration techniques (ITC, UV-Vis, and fluorometric), along with NMR and DFT calculations, we have unambiguously demonstrated that C[4]Bs form stable homoternary complexes with binding affinities ranging from 10^9 to $10^{17}\,M^{-2}$. Such ultrahigh recognition affinities in the aqueous phase are comparable to or even surpass those observed with CB[8]. Therefore, we believe that in many research and practical applications, C[4]Bs can outperform CB[8] while also offering new opportunities due to their distinct advantages. These advantages include dramatically enhanced solubility, greater ease of chemical modification, and attractive fluorescent properties. Most importantly, C[4]Bs possesses inherent chirality, enabling it to selectively differentiate chiral enantiomers and induce strong circularly polarized luminescence (CPL) with $|g_{lum}|$ values up to 1.1×10^{-2} through 1:2 complexation with achiral dyes. Moreover, high-affinity 1:2 binding is expected to enhance the detection limits of chiral sensing and the stability of CPL-active complexes, potentially enabling functionality across a broader concentration range. Therefore, we propose that C[4]Bs represents a unique chiral noncovalent connector, capable of linking two motifs with exceptional affinity within a chiral cavity in aqueous solutions. This opens up significant opportunities for chirality-related studies, such as supramolecular asymmetric catalysis, chiral supramolecular polymers, chiral supramolecular organic frameworks (cSOFs), bioimaging, and so on. Related investigations are underway in our laboratory.

https://doi.org/10.1038/s41467-025-64739-7

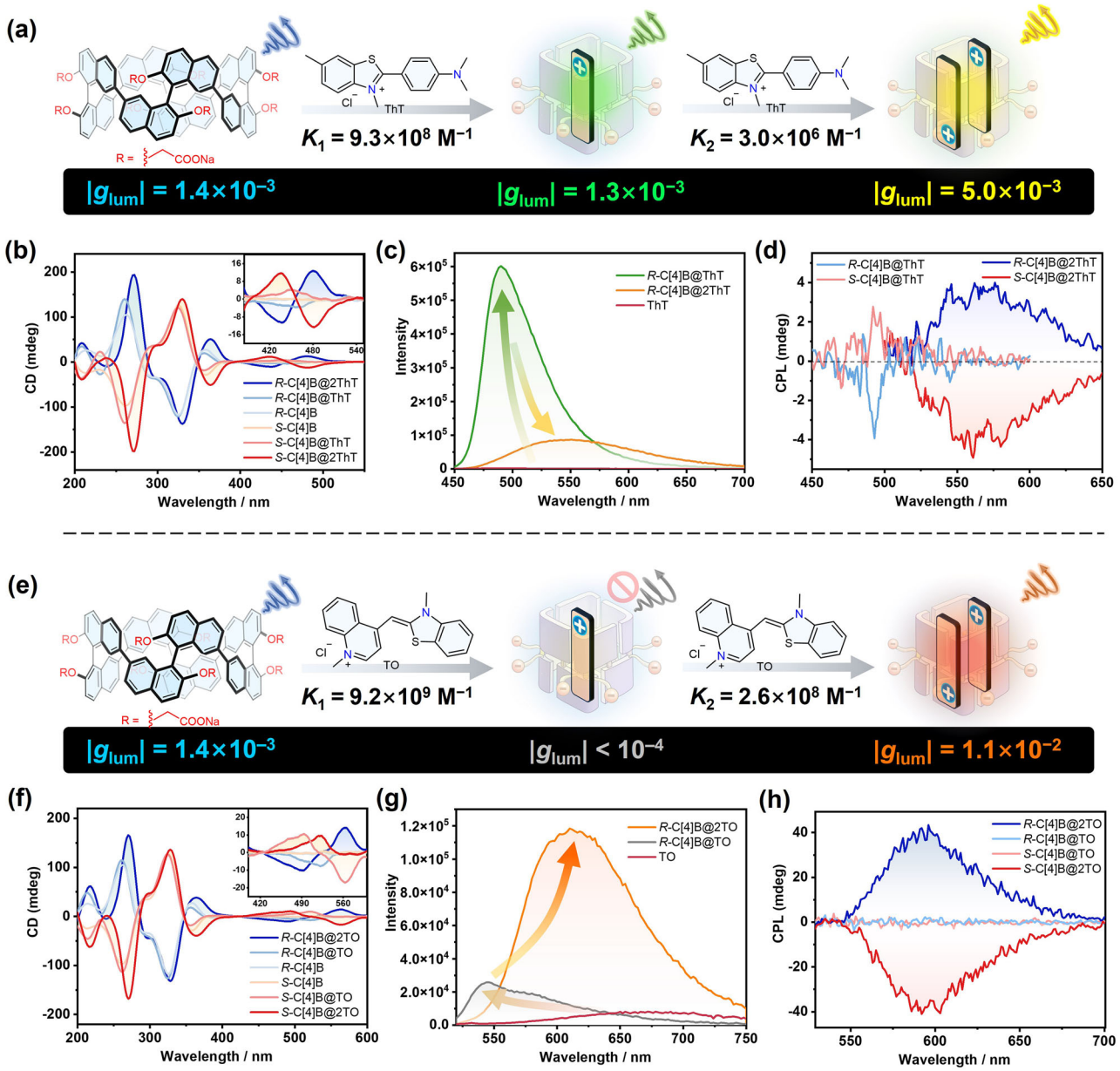

Fig. 7 | Schematic illustration and characterization of the photophysical properties of the host-guest complexes in PBS buffer solution. Formed by *R*- or *S*-C[4]B with **a**–**d** ThT or **e**–**h** TO. **b**, **f** CD spectra, **c**, **g** emission spectra, **d**, **h** CPL spectra. In (**b**, **d**, **f**, **h**), host@guest binary complexes are formed by mixing 10 μM host with 10 μM guest, host@2guest homoternary complexes are formed by mixing 10 μM host with 20 μM guest, and the concentration of free host is 10 μM. In (**c**, **g**), host@guest binary complexes are formed by mixing 10 μM guest with 12 μM host, host@2guest homoternary complexes are formed by mixing 10 μM guest with 5.0 μM host, and the concentration of free guest is 10 μM.

Methods

Chemicals

All the reagents and solvents were commercially available and used as received unless otherwise specified purification. Ni(cod)$_2$ (≥98.0%), Cod, 2,2′-bipyridine (≥99.5%) were purchased from Energy Chemical. DMF (AR), toluene (AR), sodium hydroxide (AR), methanol (AR) and sodium sulfate (AR) were purchased from Macklin Inc. THF (HPLC grade), acetonitrile (HPLC grade), were purchased from J&K Scientific. The spherical C18 silica gel column (20–45 μm, 100 Å) was obtained from Santai Chemical Technology Co., Ltd.

Synthesis procedures[60] and characterization of *RRRR- or SSSS*-corral[4]BINOL

A Schlenk tube containing Ni(cod)$_2$ (0.56 mmol), cod (0.65 mmol), 2,2′- bipyridine (0.58 mmol), DMF (0.3 ml), and toluene (0.3 ml) was stirred at 90 °C for 30 min under N_2 atmosphere. Then (*R*) or (*S*)-diethyl 2,2′-(7,7′-dibromo-[1,1′-binaphthalene]-2,2′-diyl)diacetate (0.24 mmol) dissolved in toluene (2.4 mL) was added, and the mixture was stirred at 90 °C for 24 h. After cooling to room temperature, the mixture was filtered over celite to remove the solids. The filtrate was collected and evaporated under reduced pressure, then was extracted with CH_2Cl_2 and washed with brine. The organic layers were combined, dried (Na_2SO_4), and evaporated under reduced pressure. The crude product was purified by silica gel column chromatography (CH_2Cl_2/EtOAc = 20/1) to afford a white solid. Then, Solubilized the white solid in 20% NaOH aqueous solution (1.0 ml), THF (1.0 ml), CH_3OH (1.8 ml) and stirred at 90 °C overnight, after evaporated under reduced pressure and purified by spherical C18 silica gel column chromatography (H_2O to H_2O/CH_3CN = 10/1), affording *RRRR*- or *SSSS*-C[4]BINOL as a white solid.

^{1}H NMR (400 MHz, D_2O, 298 K) of *SSSS*-C[4]BINOL: δ_H = 8.00 (d, J = 9.2 Hz, 8H), 7.73 (d, J = 8.8 Hz, 8H), 7.36 (d, J = 9.2 Hz, 8H), 7.23 (s, 8H), 7.20 (d, J = 8.5 Hz, 8H), 4.47 (d, J = 14.7 Hz, 8H), 4.36 (d, J = 14.7 Hz, 8H). ^{1}H NMR (400 MHz, D_2O, 298 K) of *RRRR*-C[4]BINOL: δ_H = 8.05 (d, J = 9.2 Hz, 8H), 7.76 (d, J = 8.5 Hz, 8H), 7.40 (d, J = 9.2 Hz, 8H), 7.25 (s, 8H), 7.22 (d, J = 8.5 Hz, 8H), 4.50 (d, J = 16.3 Hz, 8H), 4.39 (d, J = 16.3 Hz, 8H).

Apparatus

Nuclear magnetic resonance (NMR) spectra were recorded on Bruker Avance III 400 spectrometers, with working frequencies of 400 MHz for ^{1}H, and ^{1}H-^{1}H NOESY (nuclear overhauser effect spectroscopy). Chemical shifts are reported in ppm relative to the signals corresponding to the residual non-deuterated solvents (D_2O: δ_H = 4.7 ppm). UV-Vis Spectra were recorded in a quartz cell (light path 10 mm) on a Cary 100 UV-Vis spectrophotometer. CD spectra were measured on MOS-450 of BioLogic. Fluorescence spectra were recorded in a conventional quartz cell (light path 10 mm) on a Cary Eclipse fluorescence spectrometer, or spectrofluorometer Edinburgh FS5. Isothermal titration calorimetry (ITC) titration experiments were carried out on a PEAQ-ITC at 25 °C. High-resolution spectra were measured on matrix-assisted laser desorption-ionization time-of-flight mass spectrometry (MALDI-TOF MS).

Data availability

The authors declare that the data supporting the findings of this study are available within the paper and its supplementary information files or the data are available at https://doi.org/10.6084/m9.figshare.29930273. Source data containing the coordinates of optimized structures are provided.

References

1. Beatty, M. A. & Hof, F. Host–guest binding in water, salty water, and biofluids: general lessons for synthetic, bio-targeted molecular recognition. *Chem. Soc. Rev.* **50**, 4812–4832 (2021).
2. Barrow, S. J., Kasera, S., Rowland, M. J., del Barrio, J. & Scherman, O. A. Cucurbituril-based molecular recognition. *Chem. Rev.* **115**, 12320–12406 (2015).
3. Lee, J. W., Samal, S., Selvapalam, N., Kim, H.-J. & Kim, K. Cucurbituril homologues and derivatives: new opportunities in supramolecular chemistry. *Acc. Chem. Res.* **36**, 621–630 (2003).
4. Rekharsky, M. V. et al. A synthetic host-guest system achieves avidin-biotin affinity by overcoming enthalpy-entropy compensation. *PNAS* **104**, 20737–20742 (2007).
5. Shetty, D., Khedkar, J. K., Park, K. M. & Kim, K. Can we beat the biotin-avidin pair?: cucurbit[7]uril-based ultrahigh affinity host-guest complexes and their applications. *Chem. Soc. Rev.* **44**, 8747–8761 (2015).
6. Cao, L. et al. Cucurbit[7]uril·guest pair with an attomolar dissociation constant. *Angew. Chem. Int. Ed.* **53**, 988–993 (2014).
7. Montes-Navajas, P., Corma, A. & Garcia, H. Complexation and fluorescence of tricyclic basic dyes encapsulated in cucurbiturils. *ChemPhysChem* **9**, 713–720 (2008).
8. Yang, X., Wang, R., Kermagoret, A. & Bardelang, D. Oligomeric cucurbituril complexes: from peculiar assemblies to emerging applications. *Angew. Chem. Int. Ed.* **59**, 21280–21292 (2020).
9. Houk, K. N., Leach, A. G., Kim, S. P. & Zhang, X. Binding affinities of host-guest, protein-ligand, and protein-transition-state complexes. *Angew. Chem. Int. Ed.* **42**, 4872–4897 (2003).
10. Chodera, J. D. & Mobley, D. L. Entropy-enthalpy compensation: role and ramifications in biomolecular ligand recognition and design. *Annu. Rev. Biophys.* **42**, 121–142 (2013).
11. Biedermann, F., Nau, W. M. & Schneider, H. J. The hydrophobic effect revisited—studies with supramolecular complexes imply high-energy water as a noncovalent driving force. *Angew. Chem. Int. Ed.* **53**, 11158–11171 (2014).
12. Balduzzi, F. et al. A high-affinity "synthavidin" receptor for squaraine dyes. *Angew. Chem. Int. Ed.* **62**, e202314373 (2023).
13. Chen, F.-Y. et al. Expanding the hydrophobic cavity surface of azocalix[4]arene to enable biotin/avidin affinity with controlled release. *Angew. Chem. Int. Ed.* **63**, e202402139 (2024).
14. Escobar, L. & Ballester, P. Quantification of the hydrophobic effect using water-soluble super aryl-extended calix[4]pyrroles. *Org. Chem. Front.* **6**, 1738–1748 (2019).
15. Liu, W. et al. Xcage: a tricyclic octacationic receptor for perylene diimide with picomolar affinity in water. *J. Am. Chem. Soc.* **142**, 3165–3173 (2020).
16. Liu, W., Johnson, A. & Smith, B. D. Guest back-folding: a molecular design strategy that produces a deep-red fluorescent host/guest pair with picomolar affinity in water. *J. Am. Chem. Soc.* **140**, 3361–3370 (2018).
17. Liu, W. et al. Cyclophane-sustained ultrastable porphyrins. *J. Am. Chem. Soc.* **142**, 8938–8945 (2020).
18. Liu, Y., Zhou, F., Yang, F. & Ma, D. Carboxylated pillar[n]arene (n = 5-7) host molecules: high affinity and selective binding in water. *Org. Biomol. Chem.* **17**, 5106–5111 (2019).
19. Peck, E. M. et al. Rapid macrocycle threading by a fluorescent dye–polymer conjugate in water with nanomolar affinity. *J. Am. Chem. Soc.* **137**, 8668–8671 (2015).
20. Prabodh, A., Grimm, L. M., Biswas, P. K., Mahram, V. & Biedermann, F. Pillar[n]arene-based fluorescence turn-on chemosensors for the detection of spermine, spermidine, and cadaverine in saline media and biofluids. *Chem. -Eur. J.* **30**, e202401071 (2024).
21. Tang, X. et al. Self-standing chiral covalent organic framework thin films with full-color tunable guest-induced circularly polarized luminescence. *Angew. Chem. Int. Ed.* **63**, e202413171 (2024).
22. Xue, W., Zavalij, P. Y. & Isaacs, L. Pillar[n]MaxQ: a new high affinity host family for sequestration in water. *Angew. Chem. Int. Ed.* **59**, 13313–13319 (2020).
23. Zhai, C. & Isaacs, L. New synthetic route to water-soluble prism[5]arene hosts and their molecular recognition properties. *Chem. Eur. J.* **28**, e202201743 (2022).
24. Zhang, W., Bazan-Bergamino, E. A., Doan, A. P., Zhang, X. & Isaacs, L. Pillar[6] MaxQ functions as an in vivo sequestrant for rocuronium and vecuronium. *Chem. Commun.* **60**, 4350–4353 (2024).
25. Zhou, H. et al. Biomimetic recognition of quinones in water by an endo-functionalized cavity with anthracene sidewalls. *Angew. Chem. Int. Ed.* **60**, 25981–25987 (2021).
26. Yang, L. P., Wang, X., Yao, H. & Jiang, W. Naphthotubes: macrocyclic hosts with a biomimetic cavity feature. *Acc. Chem. Res.* **53**, 198–208 (2020).
27. Dong, S., Zheng, B., Wang, F. & Huang, F. Supramolecular polymers constructed from macrocycle-based host-guest molecular recognition motifs. *Acc. Chem. Res.* **47**, 1982–1984 (2014).
28. Zheng, B., Wang, F., Dong, S. & Huang, F. Supramolecular polymers constructed by crown ether-based molecular recognition. *Chem. Soc. Rev.* **41**, 1621–1636 (2012).
29. Yao, S.-Y. et al. High-affinity 1: 2 recognition based on naphthyl-azocalix[4]arene and its application as a cleavable noncovalent connector in constructing responsive supramolecular polymeric materials. *Chem. Sci.* **16**, 7066–7076 (2025).
30. Li, Z. & Yang, Y.-W. Functional materials with pillarene struts. *Acc. Mater. Res.* **2**, 292–305 (2021).
31. Ogoshi, T., Yamagishi, T. A. & Nakamoto, Y. Pillar-shaped macrocyclic hosts pillar[n]arenes: new key players for supramolecular chemistry. *Chem. Rev.* **116**, 7937–8002 (2016).
32. Chen, J. et al. Supramolecular trap for catching polyamines in cells as an anti-tumor strategy. *Nat. Commun.* **10**, 3546 (2019).

33. Hu, X.-Y., Fu, R. & Guo, D.-S. Hypoxia-responsive host–guest drug delivery system. *Acc. Mater. Res.* **4**, 925–938 (2023).
34. Liu, Y.-Y. et al. Supramolecular systems for bioapplications: recent research progress in china. *Sci. China Chem.* **67**, 1397–1441 (2024).
35. Tang, X. et al. Supramolecularly catalyzed polymerization: from consecutive dimerization to polymerization. *Angew. Chem. Int. Ed.* **57**, 8545–8549 (2018).
36. Yang, B. et al. Self-assembly of a bilayer 2D supramolecular organic framework in water. *Angew. Chem. Int. Ed.* **60**, 26268–26275 (2021).
37. Zhang, K.-D. et al. Toward a single-layer two-dimensional honeycomb supramolecular organic framework in water. *J. Am. Chem. Soc.* **135**, 17913–17918 (2013).
38. Heitmann, L. M., Taylor, A. B., Hart, P. J. & Urbach, A. R. Sequence-specific recognition and cooperative dimerization of N-terminal aromatic peptides in aqueous solution by a synthetic host. *J. Am. Chem. Soc.* **128**, 12574–12581 (2006).
39. Li, Y. et al. Adaptive chirality of an achiral cucurbit[8]uril-based supramolecular organic framework for chirality induction in water. *Angew. Chem. Int. Ed.* **60**, 6744–6751 (2021).
40. Li, Z.-T., Yu, S.-B., Liu, Y., Tian, J. & Zhang, D.-W. Supramolecular organic frameworks: exploring water-soluble, regular nanopores for biomedical applications. *Acc. Chem. Res.* **55**, 2316–2325 (2022).
41. Tian, J. et al. Three-dimensional periodic supramolecular organic framework ion sponge in water and microcrystals. *Nat. Commun.* **5**, 5574 (2014).
42. Yang, B. et al. In situ loading and delivery of short single- and double-stranded DNA by supramolecular organic frameworks. *CCS Chem.* **1**, 156–165 (2019).
43. Yu, J., Niu, J., Xu, X. & Liu, Y. Configurationally stepping confinement achieved tunable chiral near-infrared luminescence supramolecular phenothiazine organic framework. *Adv. Sci.* **11**, e2408107 (2024).
44. Du, M. & Li, C. Engineering supramolecular hydrogels via reversible photoswitching of cucurbit[8]uril-spiropyran complexation stoichiometry. *Adv. Mater.* **36**, e2408484 (2024).
45. Huang, Z. et al. Highly compressible glass-like supramolecular polymer networks. *Nat. Mater.* **21**, 103–109 (2021).
46. Wang, Z., Shui, M., Wyman, I. W., Zhang, Q.-W. & Wang, R. Cucurbit[8]uril-based supramolecular hydrogels for biomedical applications. *RSC Med. Chem.* **12**, 722–729 (2021).
47. Nguyen, H. D., Dang, D. T., van Dongen, J. L. J. & Brunsveld, L. Protein dimerization induced by supramolecular interactions with cucurbit[8]uril. *Angew. Chem. Int. Ed.* **49**, 895–898 (2010).
48. Wu, Y. et al. Cucurbit[8]uril-based water-dispersible assemblies with enhanced optoacoustic performance for multispectral optoacoustic imaging. *Nat. Commun.* **14**, 3918 (2023).
49. Yu, H. et al. Efficient intermolecular charge transport in π-stacked pyridinium dimers using cucurbit[8]uril supramolecular complexes. *J. Am. Chem. Soc.* **144**, 3162–3173 (2022).
50. Bardelang, D. et al. Cucurbit[n]urils (n= 5–8): a comprehensive solid state study. *Cryst. Growth Des.* **11**, 5598–5614 (2011).
51. Han, X.-N., Zong, Q.-S., Han, Y. & Chen, C.-F. Pagoda[5]arene with large and rigid cavity for the formation of 1 : 2 host–guest complexes and acid/base-responsive crystalline vapochromic properties. *CCS Chem.* **4**, 318–330 (2021).
52. Chen, X. Y. et al. Radically enhanced dual recognition. *Angew. Chem. Int. Ed.* **60**, 25454–25462 (2021).
53. Huang, Y.-H. et al. Dynamic metallosupramolecular cages containing 12 adaptable pockets for high-order guest binding beyond biomimicry. *J. Am. Chem. Soc.* **145**, 23361–23371 (2023).
54. Inouye, M. et al. A doubly alkynylpyrene-threaded [4]rotaxane that exhibits strong circularly polarized luminescence from the spatially restricted excimer. *Angew. Chem. Int. Ed.* **53**, 14392–14396 (2014).
55. Ruan, J. et al. Enantioselective [2+2] cross-photocycloaddition enabled by a chiral cage reactor via multilevel-selectivity control. *ACS Catal.* **14**, 7321–7331 (2024).
56. Zhang, D. et al. Photochemical graft of γ-cyclodextrin's interior leading to in-situ charge-transfer complexes with unusual regioselectivity and its application in 3D photo-printing. *Sci. China Chem.* **65**, 1149–1156 (2022).
57. Zhou, W. et al. Photo-responsive cyclodextrin/anthracene/Eu^{3+} supramolecular assembly for a tunable photochromic multicolor cell label and fluorescent ink. *Chem. Sci.* **10**, 3346–3352 (2019).
58. Sukumaran, D. P., Shoyama, K., Dubey, R. K. & Würthner, F. Cooperative binding and chirogenesis in an expanded perylene bisimide cyclophane. *J. Am. Chem. Soc.* **146**, 22077–22084 (2024).
59. Fu, R. et al. Enantiopure corral[4]BINOLs as ultrastrong receptors for recognition and differential sensing of steroids. *Angew. Chem. Int. Ed.* **63**, e202406233 (2024).
60. Fu, R. et al. A chiral emissive conjugated macrocycle for high-affinity and highly enantioselective recognition in water. *Angew. Chem. Int. Ed.* **62**, e202315990 (2023).
61. Wang, R. et al. Adaptive and ultrahigh-affinity recognition in water by sulfated conjugated corral[5]arene. *Angew. Chem. Int. Ed.* **63**, e202317402 (2024).
62. Han, H. et al. Corralarenes: a family of conjugated tubular hosts. *J. Am. Chem. Soc.* **144**, 20351–20362 (2022).
63. Huang, Z. et al. Supramolecular chemistry of cucurbiturils: tuning cooperativity with multiple noncovalent interactions from positive to negative. *Langmuir* **32**, 12352–12360 (2016).
64. Hunter, C. A. & Anderson, H. L. What is cooperativity?. *Angew. Chem. Int. Ed.* **48**, 7488–7499 (2009).
65. Mahadevi, A. S. & Sastry, G. N. Cooperativity in noncovalent interactions. *Chem. Rev.* **116**, 2775–2825 (2016).
66. Shimoyama, D. & Haino, T. Entropy-driven cooperativity in the guest binding of an octaphosphonate bis-cavitand. *Chem. Eur. J.* **26**, 3074–3079 (2020).
67. Hisano, N., Kodama, T. & Haino, T. Negative homotropic cooperativity in guest binding of a trisporphyrin double cleft. *Chem. Eur. J.* **29**, e202300107 (2023).
68. Frisch, M. J. et al. Gaussian 16 rev. B.01. Wallingford, CT (2016).
69. Humphrey, W., Dalke, A. & Schulten, K. Vmd: visual molecular dynamics. *J. Mol. Graph.* **14**, 33–38 (1996).
70. Lu, T. & Chen, F. Multiwfn: a multifunctional wavefunction analyzer. *J. Comput. Chem.* **33**, 580–592 (2012).
71. Tang, X. H. et al. Endohedral functionalization of chiral metal-organic cages for encapsulating achiral dyes to induce circularly polarized luminescence. *Chem* **7**, 2771–2786 (2021).
72. Wang, J.-Q., Han, X.-N., Han, Y. & Chen, C.-F. Advances in circularly polarized luminescence materials based on chiral macrocycles. *Chem. Commun.* **59**, 13089–13106 (2023).
73. Sun, Z., Tang, H., Wang, L. & Cao, D. Advances in chiral macrocycles: molecular design and applications. *Chem. Eur. J.* **31**, e202404217 (2025).
74. Li, T., Zhu, X., Ouyang, G. & Liu, M. Circularly polarized luminescence from chiral macrocycles and their supramolecular assemblies. *Mater. Chem. Front.* **7**, 3879–3903 (2023).
75. Takaishi, K., Maeda, C. & Ema, T. Circularly polarized luminescence in molecular recognition systems: recent achievements. *Chirality* **35**, 92–103 (2022).
76. Wang, J. et al. Selective synthesis of conjugated chiral macrocycles: sidewall segments of (–)/(+)-(12,4) carbon nanotubes with strong circularly polarized luminescence. *Angew. Chem. Int. Ed.* **59**, 1619–1626 (2019).
77. Martí-Centelles, V., Pandey, M. D., Burguete, M. I. & Luis, S. V. Macrocyclization reactions: the importance of conformational, configurational, and template-induced preorganization. *Chem. Rev.* **115**, 8736–18834 (2015).
78. Yang, C., Chen, W., Zhu, X., Song, X. & Liu, M. Self-assembly and circularly polarized luminescence from achiral pyrene-adamantane

conjugates by selective inclusion with cyclodextrins. *J. Phys. Chem. Lett.* **12**, 7491–17496 (2021).
79. Guo, Y., Han, Y., Du, X.-S. & Chen, C.-F. Chiral bishelic[6]arene-based supramolecular gels with circularly polarized luminescence property. *ACS Appl. Polym. Mater.* **4**, 3473–13481 (2022).
80. Guo, Y., Han, Y. & Chen, C.-F. Construction of chiral nanoassemblies based on host-guest complexes and their responsive cd and cpl properties: chirality transfer from 2,6-helic[6]arenes to a stilbazolium derivative. *Front. Chem.* **7**, 543 (2019).

Acknowledgements

This work is supported by the National Natural Science Foundation of China (grant nos. 22271164, U20A20259 and 22271198), the Fundamental Research Funds for the Central Universities (020-63253164, 020-63253166), Nankai University (NKU), the Strategic Priority Research Program of the Chinese Academy of Sciences (grant no. XDB1180000) and Tianshan innovation Team Plan of Xinjiang Uygur Autonomous Region, China (grant no. 2023D14002), which are gratefully acknowledged.

Author contributions

K.C. conceived and designed the project; R.F. performed systematic experiments; K.C. and R.F. integrated data and wrote the manuscript; F.Y.C. developed the calibration formula for spectral titration; L.D., H.W., and X.L. conducted high-resolution mass spectrometry for 11 host-guest complexes; F.Y.C., D.Y.L., Q.Y.Z., S.D.G., Z.H.S., L.B.J., and D.S.G. participated in data discussion and analysis. All authors read and approved the final manuscript.

Competing interests

The authors declare no competing interests.

Additional information

Supplementary information The online version contains supplementary material available at https://doi.org/10.1038/s41467-025-64739-7.

Correspondence and requests for materials should be addressed to Kang Cai.

Peer review information *Nature Communications* thanks Anthony Kermagoret-, and the other, anonymous, reviewer(s) for their contribution to the peer review of this work. A peer review file is available.